RSC Advances

ROYAL SOCIETY OF CHEMISTRY

www.rsc.org/advances

Fast formation of a novel bilayer coating with enhanced corrosion resistance and cytocompatibility on magnesium

Bo Li, Yong Han *

State Key Laboratory for Mechanical Behavior of Materials, Xi'an Jiaotong University, Xi'an 710049, China.

Abstract:

A novel bilayer coating (HT5h) composed of hydroxyapatite (HA) and MgO without any other phase components was fabricated on Mg by hydrothermal treatment (HT) of micro-arc oxidation (MAO) derived MgO in an aqueous solution containing Ca-EDTA and KH_2PO_4 for 5 h. The coating comprised an outer layer of HA nanorods with narrow interrod spacing less than 70 nm and an inner layer of MgO containing HA-sealing-pores. The adhesion strength, corrosion resistance and cytocompatibility of HT5h coating were investigated, together with the MAO-derived coating (named as MAO_0, consisting of porous MgO) and bare Mg. Adhesion strength was identified by adhesion-tension tests; corrosion resistance was determined by static immersion and electrochemical tests in phosphate buffer saline (PBS), while cytocompatibility was characterized by MTT assays and actin-nucleus staining assays of hFOB1.19 cells. The obtained results showed that both of MAO_0 and HT5h coatings possessed relatively high cohesive strengths, and HT5h coating appeared more effective than

* Corresponding author: yonghan@mail.xjtu.edu.cn (Y. Han).Tel.:+86 02982665580; fax: +86 02982663453

MAO_0 coating in protection of Mg from corrosion. Moreover, the mitochondrial activity, adhesion, and proliferation of osteoblasts were significantly enhanced on HT5h coated Mg compared to bare and MAO_0 coated Mg. The improved corrosion resistance and cytocompatibility may bring the HA and pores-sealed MgO bilayers coated Mg as Mg-based biomaterials closer to clinical reality.

Keywords: Magnesium; Bilayer coating; HA nanorods; Corrosion resistance; Cytocompatibility.

1. Introduction

Magnesium (Mg) and its alloys have been widely studied as candidate materials for orthopedics applications, due to its favorable mechanical properties for bone-fixation, low elastic modulus (41-45 GPa) well close to that of bone (3-20 GPa), which can minimize the stress shielding effect.[1-3] In addition, Mg alloys can degrade gradually *in vivo* to avoid a second surgical process and the excess of Mg ions can be excreted from urine without toxicity for human body.[4-6] Moreover, appropriate Mg ions releasing from implants can regulate signaling pathways of bone marrow stromal cells and then stimulate new bone formation.[7, 8] However, the major obstacle inhibiting their clinical use is relatively high degradation rate in physiological environment, which would lead to lose mechanical integrity prematurely and mismatch the time of fracture bone sufficiently healing.[9, 10] To overcome the demerits, many approaches have been widely investigated, in which surface modification can significantly improve corrosion resistance and biocompatibility of Mg alloys.[3, 11]

Nevertheless, the improvement endowed by the current surface modification methods is not enough to allow Mg alloys-based implants to fulfill the aim of repairing damaged tissue within 3-6 months.[1] For examples, Mg-Ca alloy with alkaline-treated coating underwent significantly corrosion after 200 h of immersion in stimulated body fluid (SBF).[12] Fluoride conversion coating on Mg alloy disappeared after 4 weeks' implantation.[13] Electrodeposition derived F-containing hydroxyapatite (F-HA) coating delaminated from Mg alloy after immersion in SBF for 4 weeks [14] and the chitosan coating fabricated by sol-gel method peeled off from Mg alloy after 10 days' immersion.[15] Microholes and cracks remained in the coatings during fabrication producers, which can act as channels for corrosion medium contacting with substrates and lead to galvanic and pitting corrosion of Mg alloy,[16] are the main reason for the unsatisfactory protective efficacy of these coatings.[12, 14, 15, 17]

Compared with the aforementioned surface modification methods derived coatings, micro-arc oxidized (MAOed) MgO coatings have shown to provide more effective protection against corrosion of Mg alloys for long-term immersion or implantation.[9, 18] Moreover, the coatings can firmly adhere to Mg substrates,[10, 19] diminishing the risk of peeling off following implantation. Unfortunately, MAOed coatings inherently possess porous structure, owing to spark discharging during MAO,[20] which seriously decreases its anti-corrosion property; thus, sealing the pores is critical for bio-application of MAO coatings. SiO_2, Al_2O_3 and ZrO_2 had been tried as sealing agents,[21, 22] while they were not biodegradable and posed the risk to induce osteolysis when exposed to bone tissue.[23]

Also, studies on chemical components of coatings have proved an enhanced role of HA in promoting adhesion, proliferation and differentiation of cells, and new bone formation compared to polymers, MgO and other inorganic components.[11, 24] Thus some researchers used electrochemical deposition to synthesize plate-like HA on MAO coatings, not only sealed the pores in MAO coatings then enhanced corrosion resistance of Mg alloys, but also stimulated new bone formation *in vivo*.[25, 26] Nevertheless, the topography of HA plays a key role in regulation of cell behavior. Our previous works showed that compared to nanogranulated TiO_2 and plate-like $Ca_{0.5}Sr_{0.5}TiO_3$, Sr-HA nanorods with narrow interrod spacing less than 70 nm significantly enhanced the adhesion, proliferation, and differentiation of osteoblast simultaneously accelerated the mineralization of extracellular matrix.[27-29] Hiromoto *et al.* hydrothermally synthesized rod-like HA coatings on Mg, and the HA coatings exhibited improved corrosion resistance *in vitro* and *in vivo* at a certain extent, but the improvement of Mg corrosion was not enough due to the intervals among the nanorods; besides, those coatings displayed weak adhesion to Mg, owing to $Mg(OH)_2$ existing between Mg substrates and HA nanorods.[24, 30, 31]

In our previous study,[10] we fabricated a bilayer coating on Mg using MAO in Ca- and P-containing electrolyte and hydrothermal treatment (HT) in a hydrothermal solution containing Ca but without P elements for 24 h. It comprised an inner layer of MgO containing pores sealed with HA nanorods and $Mg(OH)_2$ nanoplates as well as an outer layer of HA nanorods, in which the roots of the HA nanorods are embedded in the MgO matrix and the $Mg(OH)_2$ nanoplates are among the HA nanorods. This

coating showed a high adhesion strength as well as significantly improved corrosion resistance and cytocompatibility of Mg. However, the hydrothermal procedure used above took a time as long as 24 h for the formation of HA nanorods patterned outer layer; moreover, it resulted in an additional phase component $Mg(OH)_2$ to appear in the coating.

In this work, we reported our effort to shorten the formation time of HA nanorods and eliminate additional phase component $Mg(OH)_2$ by a modified hybrid approach of MAO and HT. Using the modified approach, we herein fabricated a bilayer coating composed of HA nanorods as an outer layer and HA nanorods-sealed MgO as an inner layer within 5 h of HT, and also investigated the adhesion strength, protective efficacy against phosphate buffer saline (PBS) and cytocompatibility of the coating , together with the MAO-formed porous MgO coating and bare Mg.

2. Materials and experiment methods

2.1. Micro-arc oxidation and hydrothermal treatment

For the formation of MAOed MgO coatings on pure Mg, as described in detail elsewhere,[10] commercially pure Mg discs with sizes of Φ14 × 4 mm were employed as substrates. The discs were used as anode and treated using a pulse power supply in an aqueous electrolyte containing 0.0135 M $Ca(OH)_2$, 0.125 M NaOH, and 0.02 M β-glycerophosphate disodium (β-GP) at an applied voltage of 450 V, a pulse frequency of 100 Hz, and a duty ratio of 26% for 10 min. The resultant coatings were named as MAO_0 coatings and the discs with MAO_0 coatings were termed as MAO_0

coated Mg; then a Teflon-lined autoclave was used for HT, 7.8 mL of aqueous solution containing 0.25 M $C_{10}H_{12}CaN_2Na_2O_8$ (Ca-EDTA) and 0.25 M KH_2PO_4 was added into the autoclave, adjusting pH of the solution to 8.9 by NaOH. Subsequently, a MAO_0 coated Mg disc was immersed in the solution to receive HT at 90 ℃ for 5 h. The hydrothermally treated MAO_0 coated Mg discs were marked as HT5h coated Mg.

2.3. Characterizing the microstructures and bonding strengths of the coatings

Phase identification of MAO_0 and HT5h coatings was carried out by an X-ray diffraction (X'Pert PRO, Netherland) using Cu-Kα (λ=0.15406 nm) radiation over a 2θ angle of 20-65 °at a step of 0.02 °. The morphologies and elemental compositions of the coatings were examined by a field-emission scanning electron microscope (FESEM, FEI QUANTA 600F) equipped with an energy-dispersive X-ray spectrometer (EDX). To identify the bond strengths of the coatings on pure Mg, adhesion-tension tests according to ASTM-C633 were employed. Both sides of the samples (on one side of which coatings were removed and the exposed pure Mg substrates were roughened) were attached to cylindrical steel jigs with diameter of 14 mm using E-7 glue. Tensile load was applied to each sample with an Instron type testing machine at a crosshead speed of 1 mm/min until fracture occurred. For each kind of the coated Mg, three samples were repeated and the tensile strengths were averaged. The fracture surfaces were examined with an EDX spectrometer in FESEM to determine where failure occurred.

2.4. Corrosion resistance of bare and coated Mg

Static immersion tests were carried out in phosphate buffer saline (PBS) solution, comprising 0.20 g/L KCl, 0.20 g/L KH_2PO_4, 8.00 g/L NaCl and 1.15 g/L Na_2HPO_4 at 37 ℃ according to ASTM-G31-72.[32] Bare and coated Mg discs were sealed with silastic exposing only one side to the solution. The hydrogen evolution and pH value of each sample immersed PBS solution were monitored. Potentiodynamic polarization tests of bare, MAO_0 and HT5h coated Mg discs were performed using an Autolab potentiostat set (PGSTAT, 128 N, Metrohm). Each sample with an exposing area of 1.54 cm^2 was immersed in a three electrode cell containing PBS solution to act as a working electrode. A saturated calomel electrode (SCE) was used as the reference electrode and a graphite rod as the auxiliary electrode. After a 5 min delay under open circuit conditions, the potentiodynamic polarization curves were measured from -2 to 0 V (referred to the SCE) at a scanning rate of 5 mV/s. Electrochemical impedance spectroscopy (EIS) measurements which conducted in the experimental cell mentioned above were also used to further investigate the corrosion resistance of the samples. All the EIS tests were carried out at open circuit potentials after the tested samples immersing in the PBS for 5 min. To ensure linearity in the electrode response, a small amplitude sine wave (10 mV) was applied throughout the experiments from 1 $\times 10^{-1}$ Hz to 1 $\times 10^{5}$ Hz. The impedance data were quantitatively simulated using Zview 3.1 software (U.S.A.). All the static immersion, potentiodynamic and EIS tests were performed in triplicate.

2.5. Wettability evaluation of bare and coated Mg

The hydrophilicities of bare, MAO_0 and HT5h coated Mg discs were measured by a surface contact-angle measurement machine (DSA30, Kruss, Germany). For each measurement, a 2.5 μL droplet of distilled water was suspended from the tip of the microliter syringe and the droplet was moved slowly downward to contact the sample surface, then an image was captured and the contact angle between the droplet and the sample was measured by the analysis software (DSAI). Three samples from each group were measured and two measurements were repeated at different locations of each tested sample to obtain the average.

2.6. Cytocompatibility of bare and coated Mg

Human fetal osteoblast cell line, hFOB1.19, was purchased from the Institute of Biochemistry and Cell Biology of Chinese Academy of Sciences (Shanghai, China). The cells were inoculated into complete culture medium (CCM), consisting of Dulbecco's modified Eagle medium (DMEM; HyClone, U.S.A.) supplemented with 10% fetal bovine serum (FBS; HyClone, U.S.A.), 0.3 mg/mL Geneticine418 (Sigma, U.S.A.), 0.5 mM sodium pyruvate (Sigma, U.S.A.) and 1.2 mg/L Na_2CO_3, and then incubated in a humidified atmosphere incubator with 5% CO_2 at 37 ℃. CCM was refreshed every 2 days through the incubation period.

The bare, MAO_0 and HT5h coated Mg discs were sealed with silastic, exposing only one side to CCM. The samples were placed centrally in 24-well plates, hFOB1.19 cells were seeded with a density of 8×10^4 cells/well. Fluorescence

staining of actin and cell nucleus was performed with a staining kit (Chemicon International, U.S.A.) as follows. After 24 h of culture, the cells seeded samples were fixed with 4% paraformaldehyde, permeabilized with 0.1% Triton X-100 (Sigma, U.S.A.), and washed three times with PBS buffer (PBS supplemented with 0.05% Tween-20, Sigma, U.S.A.). The cells were then incubated for 30 min at room temperature in a 1% bovine serum albumin (Sigma, U.S.A.) blocking agent. 60 ng/mL tetramethyl rhodamine isothiocyanate conjugated phalloidin were added to the cells and the cells were incubated at 37 ℃ for 60 min for actin staining. Subsequently, the cells were incubated in 0.1 μg/mL 6-diamidino-2-phenylindole at 37 ℃ for 5 min for cell nucleus staining. After each of the above-mentioned staining events, the samples were washed three times with PBS buffer. The fluorescence stained cells were analyzed with laser confocal microscopy (OLYMPUS, FV1000).

The proliferation of hFOB1.19 cells seeded on the samples was evaluated using MTT assays after 1, 3, 7 and 14 days of incubation. At the end of each time period, the CCM was removed from each well, and the samples were washed three times with PBS and then transferred to new 24-well plates. To eliminate the effects of Mg^{2+} ions on MTT solution, the cells adhered to the samples were digested using 0.5 mL 0.25% trypsin (Sigma, U.S.A.) at 37 ℃ for 10 min, whereupon 0.5 mL of CCM was added to halt digestion and consequently, cell suspensions were obtained. The cell suspensions were quickly centrifuged and resuspended in 250 μL fresh CCM, and then, the cells were reseeded in new 48-well plates and incubated for another 24 h to allow the cells to fully attach in order to facilitate MTT assays. Following removal of

CCM from each well and washing three times with PBS, 15 μL of MTT (Sigma, U.S.A.) solution (5 mg/mL MTT in PBS) was added with 250 μL of CCM and cultured for 4 h. The medium was subsequently removed and 100 μL of dimethyl sulfoxide (DMSO; Sigma, U.S.A.) was added to each well and oscillated for 10 min. The resulting DMSO solution was transferred to new 96-well plates and the absorbance was measured at 490 nm. Four specimens from each group were tested, and each test was repeated four times (n=4). After 1 and 3 days of cultivation, the cells adhered on the samples were washed with PBS for three times, and fixed with 2.5% glutaraldehyde for 1 h at 4 ℃. The cell-fixed samples were then dehydrated in ethanol, followed by vacuum drying. After gold-palladium coating, the samples were observed under FESEM for cell morphologies.

The data were analyzed using SPSS 16.0 software (SPSS, U.S.A.). One-way ANOVA and the Student-Newman-Keuls post hoc test were used to determine the level of significance. $p < 0.05$ was considered to be significant, and $p < 0.01$ was considered to be highly significant.

3. Results and Discussion

3.1. Phase components and microstructures of MAO_0 and HT5h coatings

The phase components of MAO_0 coating before and after HT for 5 h in an aqueous solution containing Ca-EDTA and KH_2PO_4 are shown in Fig. 1. MAO_0 coating composes a single phase of MgO. After HT for 5 h, a new phase component of $Ca_{10}(PO_4)_6(OH)_2$ (*e.g.* HA) appears as identified by XRD peaks at 25.85, 31.73,

46.80 and 49.51 ° according to ICDD card no. 9-432, indicating the HT5h coating consists of MgO and HA, without additional phase component $Mg(OH)_2$ generating during HT. Surface and cross-sectional morphologies of MAO_0 and HT5h coatings are shown in Fig. 2. As shown in Fig. 2a, MAO_0 coating is porous and these micropores distribute homogeneously with diameter of 2-3 μm. The thickness of the coating is about 15 μm, as identified by EDX cross-sectional profiles of Mg, Ca, and P, distributing uniformly in MAO_0 coating; numerous pores generated by micro-arc discharge run through the entire coating (right image in Fig. 2a). Noticeably, both surface and cross-sectional views exhibit a smooth and dense structure of MAO_0 coating, and no discontinuities can be found between the substrate and coating. After HT for 5 h, surface of the resultant HT5h coating is fully covered with the nanorod crystals composed of HA as confirmed by XRD (Fig. 1). The HA nanorods show randomly oriented and homogeneously distributed with a mean diameter of 83.6 ± 2.55 nm, length of 633.3 ± 15.28 nm and interrod spacing of 60.7 ± 2.51 nm; moreover, HA nanorods also form on walls of the pores to further seal them (as supported by the magnified view in circle-marked area in right image of Fig. 2b). The EDX profiles of Ca, P, and Mg on the magnified cross-section of HT5h coating are shown in right image of Fig. 2b, revealing clearly that HT5h coating consists of two-layers with HA nanorods as an outer layer and HA nanorods-sealed MgO as an inner layer adjacent to Mg substrate.

The formation of HA nanorods in Ca-EDTA and KH_2PO_4 contained hydrothermal solution with pH value of 8.9 at 90 ℃ can be described as follows:

during HT, sufficient Ca^{2+} dissociated from Ca-EDTA, as well as the PO_4^{3-} transferred from the reaction between $H_2PO_4^-$ and OH^- in the solution reach the critical concentrations, becoming supersaturated with respect to HA, subsequently the appropriate pH value at which the HA crystals are stable [30] triggers the crystal nucleation and growth according to the equation: $10Ca^{2+} + 6PO_4^{3-} + 2OH^- \rightarrow Ca_{10}(PO_4)_6(OH)_2$.[33] Due to the high density of nuclei, the HA crystals grow in length into nanorods at *c*-axis direction with prolonging HT time.[31] Meanwhile, hydrothermal solution can easily penetrate into the pores of MAO-derived porous MgO layer, then HA nanorods form in the pores and further seal them. In addition, no $Mg(OH)_2$ forms in the bilayer coating during HT, which is attributed to the higher nucleation rates of HA than that of $Mg(OH)_2$. The nucleation rates of HA and $Mg(OH)_2$ are determined by their solubility and the concentration of Ca^{2+} in hydrothermal solution.[31, 34, 35] It has been reported that the solubility of HA and $Mg(OH)_2$ in water are 1.3×10^{-6} mol/L and 1×10^{-1} mol/L, respectively, and the lower solubility of HA would promote the nucleation of HA much more frequently than the $Mg(OH)_2$ formation.[34] Furthermore, Ca^{2+} can be sufficiently provided by hydrothermal solution with high concentration of Ca-EDTA to accelerate the formation of HA nucleus.[35] Herein, HA nucleus can be quickly formed and grow in length to cover and seal the porous MgO layer, which inhibits the solution to contact with MgO and avoids the formation of $Mg(OH)_2$ in the bilayer coating.

3.2. Bonding strengths of MAO_0 and HT5h coatings

In adhesion-tension test, tensile strength is used to character the bonding strength of a coating, either the cohesive strength of the coating or the adhesive strength between the coating and substrate, depending on the failure occurs in the interior of the coating or at the interface of the coating and substrate. Bonding strengths of MAO_0 and HT5h coatings are 19.43 ± 1.05 MPa and 16.3 ± 1.94 MPa, respectively. Bonding strength of the bilayer coating fabricated in our previous study [10] is 17.65 ± 2.39 MPa (measured by adhesion-tension test and not shown in that work). Compared to the hybrid method in our previous study, the modified hybrid approach of MAO and HT has little influence on bonding strength of the bilayer coating. To determine where failure happens, surface morphologies and element components of a couple of fracture surfaces on the tested sample and steel jig are examined, as shown in Fig. 3. For MAO_0 coated Mg, the pores in MgO layer (Fig. 2a) still can be observed, the characteristic Ca and P elements distributing throughout the entire MgO layer (Fig. 2a) can also be detected on both sides of sample and steel jig and have similar contents, revealing that the tensile fracture occurs in the interior of the porous MgO layer. Moving to HT5h coated Mg, fewer micro-pores can be seen on both sample and steel jig sides compared to that in MAO_0 coated Mg, which is attributed to the sealing effect of HA nanorods (Fig. 2b); the Ca and P elements also can be detected on both sides, and the Ca and P contents are slightly higher on jig side than that on sample side, which may attribute to the fact that the contents of Ca and P in the nanorod-HA layer are much higher than those in the sealed MgO layer (EDX spectra in Fig. 2b). Except for Ca and P, Mg element which is exclusive in nanorod-HA layer still can be

detected on jig side, suggesting that the tensile fracture also occurs in the interior of sealed MgO layer in HT5h coating, rather than the upper nanorod-HA/sealed MgO interface. Noticeably, the Ca/P atomic ratios detected on the sample and the jig sides for HT5h coated Mg are 0.35 and 0.66, respectively, which are much lower than the stoichiometric HA (1.67). Due to the tensile fracture position, EDX gives the relative elemental compositions in the interior of the sealed MgO layer, in which the Ca/P ratio is mainly determined by the Ca and P elements incorporated in MAO-derived MgO layer rather than that in HT-derived HA. Moreover, as proved by the EDX on the tensile fracture surfaces of MAO_0 coating, the Ca/P ratio in the MgO layer is quite low (~0.25), resulting in the lower ratios than the stoichiometric HA on the fracture surfaces of HT5h coating. However, the ratios detected on the fracture surfaces of HT5h coating are slightly higher than those on the fracture surfaces of MAO_0 coating, which is attributed to the HT-derived HA nanorods contained in the micropores and the upper layer. Herein, the results of adhesion-tension tests reflect the cohesive strengths of MAO_0 and HT5h coatings, and the adhesive strengths between the coatings and substrates are much higher; furthermore, the adhesion strength between the upper nanorod-HA layer and pore-sealed MgO layer is also higher than the cohesive strength of MgO layer in HT5h coating, indicating that HT5h coating can be used as a protective coating with high bonding strength.[36] Noticeably, HT results in a slight decrease in cohesive strength of the MgO layer, due to the migration of PO^{3-} and Ca^{2+} in the layer during HT.[10, 19]

3.3. Corrosion resistance of bare and coated Mg

Fig. 4a exhibits H_2 evolution from bare, MAO_0 and HT5h coated Mg discs during immersion tests. Following immersion for the same duration, the amount of H_2 releasing from the immersed HT5h coated Mg discs is the smallest among the bare and coated Mg discs, even cannot be detected during the initial hours of immersion. As known, $Mg + 2H_2O \rightarrow Mg(OH)_2 + H_2$, thus the H_2 evolution can be used to character the degradation of Mg substrate and its derived $Mg(OH)_2$ amount. According to ASTM-G31-72,[32] the corrosion rates of bare Mg and the Mg substrates underlying MAO_0 and HT5h coatings calculated from the volume of H_2 evolution are about 1.17, 0.32 and 0.093 mg cm^{-2} day^{-1}, respectively. MAO_0 and HT5h coatings can reduce the corrosion rates of the underlying Mg substrates by 72.6% and 92.1%, respectively. However, previous studies [18] showed that about 50-80% reduction in corrosion rates of Mg alloy substrates can be obtained by other surface modification derived coatings, such as polymer coatings, electrodeposition coatings, alkaline-treated coatings and fluoride convention coatings. This result reveals that more effective protection can be provided to Mg substrate against corrosion by HT5h coating than the aforementioned other coatings. Furthermore, the smallest amount of H_2 releasing from HT5h coated Mg reflects that Mg degradation derived $Mg(OH)_2$ is less in amount than MAO_0 coated Mg and far less than bare Mg. More $Mg(OH)_2$ formed in MAO_0 coated Mg is attributed to the numerous pores in MAO_0 coating, which will act as channels to enable the corrosive medium to penetrate into the coating and onto Mg substrate, leading to generate more $Mg(OH)_2$ in the pores and at

the interface of MgO and Mg. Nevertheless, the pores are sealed with HA nanorods in HT5h coating (Fig. 2a), inhibiting penetration of the corrosive medium into the coating and onto substrate. As known, the molar volume of $Mg(OH)_2$ is larger than MgO, which will induce stress in the coating then develop cracks within MgO and at MgO/Mg interface.[37] Subsequently, the cracks at the MgO/Mg interface will weak the adhesion of the coating to Mg, resulting in delamination of the coating and server pitting corrosion on the substrate which leads to the premature loss of mechanical integrity.[10, 38] Thus compared to MAO_0 coating, less amount of cracks will develop within MgO and at MgO/Mg interface in HT5h coating due to less $Mg(OH)_2$ formed, also it can be deduced that HT5h coated Mg can keep mechanical integrity for longer time.

Besides H_2 evolution, the degradation of the coatings and underlying Mg can also alter the pH values of the samples immersed solution, as shown in Fig. 4b. The pH values of the coated Mg immersed solution are lower compared with bare Mg immersed solution at each immersion time point, especially for HT5h coated Mg immersed solution. After immersion for 15 days, pH value of HT5h coated Mg immersed PBS is 8.16, in contrast the pH values of bare and MAO_0 coated Mg immersed PBS increase to 11.53 and 9.61, respectively. This phenomenon is attributed to the degradation of Mg and MgO can be retarded by the HA nanorods in HT5h coating. The results of H_2 evolution and alkalization of the PBS immersing the samples indicate that HT5h coating can provide longer term protection to underlying Mg substrate from severe corrosion compared to MAO_0 coating.

The potentiodynamic polarization (PDP) curves of bare and coated Mg discs tested in PBS are shown in Fig. 5a, and the corrosion potentials (E_{corr}) and corrosion current densities (i_{corr}) of the samples can be drawn from the PDP curves as summarized in Table 1. Compared to bare and MAO_0 coated Mg discs, HT5h coated Mg exhibits five orders and two orders of magnitude decrease in i_{corr}, meanwhile, HT5h coated Mg is ennobled in E_{corr}.

EIS tests are also carried out to further character the protective efficacy of the coatings. The Nyquist plots drawn from the impedance spectra of the bare and coated Mg discs tested in PBS are shown in Fig. 5b. The plots of the coated Mg display two capacitance loops: one is at high frequency and another is at the low frequency, which are associated with the PBS penetrating into the coatings and Faradic charge transfer reaction at the interfaces of the coatings and substrates, respectively.[39-41] Different from the coated Mg, the bare Mg only shows one loop in the plot which reflects the charge transfer reaction at the interface of solution and Mg substrate. The impedance spectra observed for bare and coated Mg are fitted using the equivalent circuit as shown in Fig. 5c. In which, Rs is the resistance of tested PBS; R_b and Q_b are the charge transfer resistance and capacitance of electric double layer at Mg/PBS interface, respectively; Q_{dl} and R_{ct} represent the capacitance of electric double layer and charge transfer resistance at the interface of coating and substrate; Q_{po} and R_{po} are the capacitance and solution penetration resistance of the tested coating. Furthermore, Fig. 5b also indicates that the fitted data from the equivalent circuits are in good agreement with the experimental data, with deviation less than 5%.

The fitting results are summarized in Table 1. The bare and coated Mg tested solutions have similar Rs values, which is attributed to the fixed components of the medium and position between the tested samples and reference electrode during tests. Noticeably, R_{po} value of HT5h coated Mg is about two orders larger than that of MAO_0 coated Mg, revealing that the sealing agent of HA nanorods in the pores of MAOed MgO can significantly inhibit penetration of the corrosive medium into the coatings. Meanwhile, R_{ct} value of HT5h coated Mg is three orders of magnitude larger compared with that of MAO_0 coated Mg, giving further proof of better corrosion resistance of HT5h coating. The static immersion, potentiodynamic and EIS tests suggest that HT5h coating comprising an inner layer of MgO containing HA -sealing-pores as well as an outer layer of narrow spaced HA nanorods is a superior protective barrier for Mg substrate.

3.4. Wettability of bare and coated Mg

The wettability of a bone implant is known to play important role in biological tissue response. The contact angles of water droplets on bare, MAO_0 and HT5h coated Mg discs are 83.8 ° ± 3.01 °, 49.6 °± 3.09 ° and 15.1 ° ± 0.59 °, respectively, as shown in Fig. 6, suggesting that HT5h coating exhibits much better hydrophilicity than bare Mg and MAO_0 coating. Whereupon the enhanced adhesion and proliferation of osteoblast on HT5h coated Mg can be expected.[28]

3.5. Cytocompatibility of bare and coated Mg

To identify the adhesion and binding response of osteoblast on bare and coated Mg, actin-nucleus two-colors staining fluorescence images with different magnifications of osteoblast after 24 h seeding on the samples are displayed in Fig. 7. Compared to bare Mg, the cells cultured on the coated Mg show health and normal morphologies, especially on the HT5h coated Mg. Furthermore, markedly more cells are observed on the surface of HT5h coated Mg (denoted by nucleus) than the bare and MAO_0 coated Mg groups. The individual cell on HT5h coated Mg significantly spreads with increased area, furthermore, thicker and better organized filamentous actin bundles which extending in numerous directions can be observed, indicating that the osteoblast are more favorable for adhering and spreading on HT5h coated Mg.

MTT assays are carried out to character the mitochondrial activity of the cells seeded on bare and coated Mg after 1, 3, 7 and 14 days of incubation, as shown in Fig. 8a. On day 1, the mitochondrial activity of cells is very low on bare Mg and even cannot be detected on day 3. However, the viability of cells on the coated Mg are significantly enhanced, especially on HT5h coated Mg. With prolonging incubation time, the mitochondrial activity of cells on MAO_0 and HT5h coated Mg tends to increase, indicating the cell proliferation occurs after one day of incubation on them. However, there is an obvious difference in proliferation of cells on the coated Mg at each time point. Cell proliferation on HT5h coated Mg shows significant increase compared to that on MAO_0 coated Mg, revealing that HT5h coating is more suitable for cell adhesion and proliferation. As represents, the morphologies of cells after 1 and 3 days of incubation on bare and coated Mg are displayed in Fig. 8b-g. After 1

day of incubation, small amount of cells adhere onto bare Mg, which are spherically shaped and spread less, in addition many cracks appear on the surface due to the fast degradation of Mg. In contrast, no obvious changes on the surface of coated Mg can be found, indicating better corrosion resistance of the coatings in CCM, which is in accord with the results of immersion and electrochemical tests (Fig. 4 and 5); moreover, the cells cultured on coated Mg exhibit polygonal shape with increased spreading areas, especially for HT5h coated Mg, which is consistent with the actin-nucleus staining results (Fig. 7). Furthermore, many dense lamellipodia and filopodia stretching out to anchor to HT5h coating surface (magnified image in Fig. 8f), forming better intercellular connection, and enhancing cell-cell communication, which can coordinate cellular responses to external signals and regulate osteoblast differentiation.[42, 43] On day 3, no survival cells can be found on the surface of bare Mg, keeping with the result of MTT assay, and the cracks on the surface are widened. However, the cells cultured on the coated Mg increase in amount and spread very well, especially on HT5h coated Mg, nearly covering the whole surface.

As osteoblast is an anchorage-dependent cell, cytocompatibility of bare and coated Mg relies on two key factors: the culture medium in which the cells locate (such as pH value, H_2 concentration, *etc.*) and the surface features of a material to which the cells adhere (such as chemical composition and topography, *etc.*).[10] For the culture medium, it has been reported appropriate amount of H_2 contained in culture medium can significantly enhance ALP activity of the pre-osteoblast and keep viability of the cells above 90%,[44] however, excessive H_2 would lead to cell damage

and inhibit fracture bone healing.[45] Regarding to pH value of culture medium, osteoblast viability was found to be enhanced with increasing pH up to 8-8.5,[46] but when the pH value was higher than 10.5, adhesion and proliferation of cells were retarded.[47] Cipriano *et al.* [48] also found that adhesion density of bone marrow derived mesenchymal stem cells significantly decreased with pH value up to 9.5. The results in this work show that cell viability is quite low on bare Mg, even no cells survive after 3 days of cultivation, which is related to huge amount of H_2 releasing (Fig. 4a) and strong alkalization as a result of fast corrosion (Fig. 4b). As a comparison, more cells adhere onto the surfaces of MAO_0 and HT5h coated Mg, meanwhile the mitochondrial activity and proliferation of the cells are enhanced, in which the best osteoblastic cytocompatibility is achieved with HT5h coated Mg due to the better protective efficiency of HT5h coating and consequent decreased hydrogen evolution and alkalization. At the same time, surface hydrophilicity, chemical component and topography of the coatings also play key roles to influence cell behavior. Previous studies have shown that hydrophilic surface could absorb more RGD (arginine-glycine-aspartic acid)-contained anchoring proteins such as vitronectin (Vn) and fibronectin (Fn) from serum-containing medium to form more bioactive conformation for cell adhesion.[49] Furthermore, compared to polymers, MgO, and other inorganic components, HA can significantly enhance adhesion, proliferation and differentiation of cells.[3, 11, 24, 25] Our previous studies also give the proof that the topography of HA can regulate cell behavior directly. For example, Sr-HA nanorods with narrow interrod spacing less than 70 nm can significantly enhance adhesion and

proliferation of osteoblast compared to nanogranulated TiO_2 and Sr-HA.[27-29] Therefore, HT5h coating with narrow interrod spaced HA nanorods which has a superior hydrophilicity as an outer layer in conjunction with pore-sealed MgO as an inner layer exhibits particularly good cytocompatibility.

4. Conclusions

A novel bilayer coating (HT5h) composed of hydroxyapatite (HA) and MgO without any other phase components was fabricated on Mg by hydrothermal treatment (HT) of micro-arc oxidation (MAO) derived MgO in an aqueous solution containing Ca-EDTA and KH_2PO_4 for 5 h. The coating comprises an inner layer of MgO containing pores sealed with HA nanorods and an outer layer of narrow interrod spaced HA nanorods. We characterized the bonding strengths of the MAO-formed porous MgO (terms as MAO_0) and HT5h coatings using adhesion-tension method. The tensile fractures occurred in the interior of the MgO layers in MAO_0 and HT5h coatings, rather than the MgO/Mg interfaces for MAO_0 and HT5h coatings or HA/MgO interface for HT5h coating, suggesting that the tensile results reflected the cohesive strengths of the coatings, and both of the coatings exhibited relatively high cohesive strengths. Hydrogen evolution and pH changes of the PBS solution immersing the bare and coated Mg revealed that the HT5h coating showed better improvement of Mg corrosion resistance performance over the MAO_0 coating. Electrochemical measurements also demonstrated that the HT5h coated Mg had a significant advantage over bare and MAO_0 coated Mg in anti-corrosion behavior.

Moreover, compared to the bare and MAO_0 coated Mg, HT5h coated Mg was shown to greatly enhance the mitochondrial activity, adhesion, and proliferation of osteoblast.

Acknowledgements

We appreciate the National Program on Key Basic Research Project (973 Program) of China (Grant number 2012CB619103) and National Natural Science Foundation of China (Grant No. 51371137, 51071120) for financially supporting this work.

References

1 M. P. Staigera, A. M. Pietaka and J. Huadmaia, *Biomaterials*, 2006, **27**, 1728-1734.

2 Y. J. Chen, Z. G. Xu, C. Smith and J. Sankar, *Acta Biomater.*, 2014, **10**, 4561-4573.

3 H. Hornberger, S. Virtanen and A. R. Boccaccini, *Acta Biomater.*, 2012, **8**, 2442-2455.

4 N. Erdmann, N. Angrisani, J. Reifenrath, A. Lucas, F. Thorey and D. Bormann, *Acta Biomater.*, 2011, **7**, 1421-1428.

5 H. Hermawan, D. Dubé and D. Mantovani, *Acta Biomater.*, 2010, **6**, 1693-1697.

6 D. Dziuba, A. Meyer-Lindenberg, J. M. Seitz, H. Waizy, N. Angrisani and J. Reifenrath, *Acta Biomater.*, 2013, **9**, 8548-8560.

7 S. Yoshizawa, A. Brown, A. Barchowsky and C. Sfeir, *Acta Biomater.*, 2014, **10**, 2834-2842.

8 H. M. Wong, S. L. Wu, P. K. Chu, S. H. Cheng, K. D. K. Luk, K. M. C. Cheung and K. W. K. Yeung, *Biomaterials*, 2013, **34**, 7016-7032.

9 T. Imwinkelried, S. Beck, T. Iizuka and B. Schaller, *Acta Biomater.*, 2013, **9**, 8643-8649.

10 B. Li, Y. Han and K. Qi, *ACS Appl. Mater. Interfaces*, 2014, **6**, 18258-18274.

11 Y. F. Zheng, X. N. Gu and F. Witte, *Mater. Sci. Eng., R*, 2014, **77**, 1-34.

12 X. N. Gu, W. Zheng, Y. Cheng and Y. F. Zheng, *Acta Biomater.*, 2009, **5**, 2790-2799.

13 F. Witte, J. Fischer, J. Nellesen, C. Vogt, J. Vogt, T. Donath and F. Beckmann, *Acta Biomater.*, 2010, **6**, 1792-1799.

14 Y. Song, S. Zhang, J. Li, C. Zhao and X. Zhang, *Acta Biomater.*, 2010, **6**, 1736-1742.

15 X. N. Gu, Y. F. Zheng, Q. X. Lan, Y. Cheng, Z. X. Zhang, T. F. Xi and D. Y. Zhang, *Biomed. Mater.*, 2009, **4**, 044109-044112.

16 J. F. Zhang, W. Zhang, C. W. Yan, K. Q. Du and F. H. Wang, *Electrochim. Acta*, 2009, **55**, 560-571.

17 H. M. Wong, K. W. Yeung, K. O. Lam, V. Tam, P. K. Chu, K. D. Luk and K. M. Cheung, *Biomaterials*, 2010, **31**, 2084-2096.

18 X. N. Gu, N. Li, W. R. Zhou, Y. F. Zheng, X. Zhao, Q. Z. Cai and L. Q. Ruan, *Acta Biomater.*, 2011, **7**, 1880-1889.

19 Y. Han, J. H. Zhou, L. Zhang and K. W. Xu, *Nanotechnology*, 2011, **22**, 275603-275613.

20 H. H. Luo, Q. H. Cai, B. K. Wei, B. Yu, D. J. Li, H. He and Z. Liu, *J. Alloys Compd.*, 2008, **464**, 537-543.

21 H. P. Duan, K. Q. Du, C. W. Yan and F. H. Wang, *Electrochim. Acta*, 2006, **51**, 2898-2908.

22 W. Shang, B. Z. Chen, X. C. Shi, Y. Chen and X. Xiao, *J. Alloys Compd.*, 2009, **474**, 541-545.

23 Y. P. Jiang, T. H. Jia, W. M. Gong, P. H. Wooley and S. Y. Yang, *Acta Biomater.*, 2013, **9**, 7564-7572.

24 S. Hiromoto, M. Inoue, T. Taguchi, M. Yamane and N. Ohtsu, *Acta Biomater.*, 2015, **11**, 520-530.

25 S. Chen, S. K. Guan, W. Li, H. X. Wang, J. Chen, Y. S. Wang and H. T. Wang, *J. Biomed. Mater. Res., B*, 2012, **100B**, 533-543.

26 Q. Zhao, X. Guo, X. Dang, J. Hao, J. Lai and K. Wang, *Colloids Surf., B*, 2013, **102**, 321-326.

27 Y. Han, J. H. Zhou, S. M. Lu and L. Zhang, *Rsc Adv.*, 2013, **3**, 11169-11184.

28 J. H. Zhou, B. Li, S. M. Lu, L. Zhang, and Y. Han, *Acs Appl. Mater. Interfaces*, 2013, **5**, 5358-5365.

29 J. H. Zhou, Y. Han and S. M. Lu, *Int. J. Nanomed.*, 2014, **9**, 1243-1260.

30 M. Tomozawa and S. Hiromoto, *Acta Mater.*, 2011, **59**, 355-363.

31 S. Hiromoto and M.Tomozawa, *Surf. Coat. Technol.*, 2011, **205**, 4711-4719.

32 ASTM. Standard Practice for Laboratory Immersion Corrosion Testing of Metals, ASTM-G31−72, American Society for Testing and Materials: Philadelphia, PA,

2004.

33 H. X. Wang, S. K. Guan, X. Wang, C. X. Ren and L. G. Wang, *Acta Biomater.*, 2010, **6**, 1743-1748.

34 M. Tomozawa and S. Hiromoto, *Appl. Surf. Sci.*, 2011, **257**, 8253-8257.

35 M. Tomozawa, S. Hiromoto and Y. Harada, *Surf. Coat. Technol.*, 2010, **204**, 3243-3247.

36 B. D. Hahn, J. M. Lee, D. S. Park, J. J. Choi, J. Ryu, W. H. Yoon, B. K. Lee, D. S. Shin and H. E. Kim, *Thin Solid Films*, 2010, **518**, 2194-2199.

37 J. Liang, P. B. Srinivasan, C. Blawert, M. Stormer and W. Dietzel, *Electrochim. Acta*, 2009, **54**, 3842-3850.

38 X. Lin, X. M. Yang, L. L. Tan, M. Li, X. Wang, Y. Zhang, K. Yang, Z. Q. Hu and J. H. Qiu, *Appl. Surf. Sci.*, 2014, **288**, 718-726.

39 D. Song, A. B. Ma, J. H. Jiang, P. H. Lin, D. H. Yang and J. F. Fan, *Corros. Sci.*, 2011, **53**, 362-373.

40 G. Song, A. Atrens, D. S. John, X. Wu and J. Nairn, *Corros. Sci.*, 1997, **39**, 1981-2004.

41 Y. J. Zhang, C. W. Yan, F. H. Wang and W. F. Li, *Corros. Sci.*, 2005, **47**, 2816-2831.

42 P. C. Schiller, G. D'Ippolito, W. Balkan, B. A. Roos and G. A. Howard, *Bone*, 2001, **28**, 38-44.

43 R. Civitelli, *Arch. Biochem. Biophys.*, 2008, **473**, 188-192.

44 H. M. Wong, Y. Zhao, V. Tam, S. L. Wu, P. K. Chu, Y. F. Zheng, M. K. T. To, F. K.

L. Leung, K. D. K. Luk, K. M. C. Cheung and K. W. K. Yeung, *Biomaterials*, 2013, **34**, 9863-9876.

45 X. B. Chen, D. R. Nisbet, R. W. Li, P. N. Smith, T. B. Abbott, M. A. Easton, D. H. Zhang and N. Birbilis, *Acta Biomater.*, 2014, **10**, 1463-1474.

46 Y. H. Shen, W. C. Liu, C. Y. Wen, H. B. Pan, T. Wang, B. W. Darvell, W. W. Lu and W. H. Huang, *J. Mater. Chem.*, 2012, **22**, 8662-8670.

47 L. P. Xu, F. Pan, G. N. Yu, L. Yang, E. L. Zhang and K. Yang, *Biomaterials*, 2009, **30**, 1512-1523.

48 A. F. Cipriano, A. Sallee, R. G. Guan, Z. Y. Zhao, M. Tayoba, J. Sanchez and H. N. Liu, *Acta Biomater.*, 2015, **12**, 298-321.

49 R. Huang, Y. Han and S. M. Lu, *Colloids surf., B*, 2013, **111**, 232-241.

Tables and Figures captions

Table 1 Corrosion potentials (E_{corr} Values) and corrosion current densities (i_{corr} Values) obtained from the polarization curves of bare and coated Mg discs and EIS fitted parameters of the equivalent circuits for bare and coated Mg discs in PBS solution.

Fig. 1 XRD patterns detected on the surface of MAO_0 coating before and after HT for 5 h.

Fig. 2 SEM surface and cross-sectional morphologies of the MAO_0 coating before (a) and after HT for (b) 5 h; the insets are corresponding magnified images of the dotted marked areas.

Fig. 3 SEM morphologies as well as EDX spectra and elements contents (right insets)

taken from the dotted-squared areas of the tensile fracture surfaces examined on (a, b) MAO_0 and (c, d) HT5h coated Mg; (a, c) the samples sides and (b, d) the steel jigs sides.

Fig. 4 (a) Hydrogen volumes released by bare and coated Mg in PBS solution and (b) pH values of the PBS solution immersing bare and coated Mg as a function of immersion time.

Fig. 5 (a) Polarization curves and (b) Nyquist plots of EIS spectra of bare and coated Mg discs measured in PBS solution, (c) equivalent circuits used to fit the impedance data of bare and coated Mg discs.

Fig. 6 Hydrophilicity of (a) bare, (b) MAO_0 and (c) HT5h coated Mg.

Fig. 7 Actin (red) and cell nucleus (blue) fluorescence images with different magnifications of osteoblast after 24 h of culture on bare Mg as well as MAO_0, and HT5h coated Mg.

Fig. 8 (a) MTT assay of osteoblast incubated on bare and the coated Mg for 1, 3, 7 and 14 days; SEM morphologies of osteoblast cultured on bare (b, c), MAO_0 (d, e) and HT5h (f, g) coated Mg for 1 day (b, d and f) and 3 days (c, e and g). Data are presented as the mean ± SD, n = 4, (**) $p < 0.01$ compared with the bare Mg, and (++) $p < 0.01$ compared with the MAO_0 coated Mg.

Table 1 Corrosion potentials (E_{corr} Values) and corrosion current densities (i_{corr} Values) obtained from the polarization curves of bare and coated Mg discs and EIS fitted parameters of the equivalent circuits for bare and coated Mg discs in PBS solution.

Samples	Bare Mg	MAO_0 coated Mg	HT5h coated Mg
E_{corr} (V vs. SCE)	-1.49	-1.45	-1.43
i_{corr} (A/cm^2)	1.52×10^{-3}	4.06×10^{-6}	2.80×10^{-8}
R_s(Ω)	33.96	44.84	33.98
R_{po} (Ωcm^2)	-	4.63×10^{3}	5.46×10^{5}
Q_{po} ($\mu F\ cm^{-2}$)	-	9.48×10^{-6}	1.05×10^{-7}
n_{po}	-	0.8584	0.8122
R_b (Ωcm^2)	1.28×10^{3}	-	-
Q_b ($\mu F\ cm^{-2}$)	1.186×10^{-5}	-	-
n_b	0.933	-	-
R_{ct} (Ωcm^2)	-	9.59×10^{2}	2.18×10^{5}
Q_{dl} ($\mu F\ cm^{-2}$)	-	6.74×10^{-4}	2.83×10^{-6}
n_{dl}	-	0.9283	0.8

Table of Content

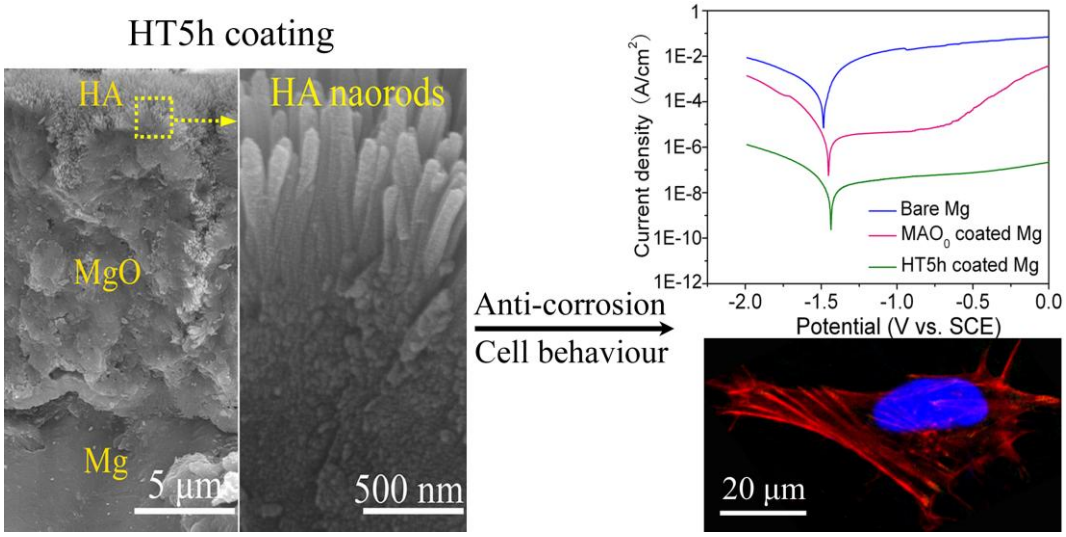

A bilayer coating on magnesium provides effective protection to substrate from corrosion and facilitates osteoblast adhesion and proliferation.

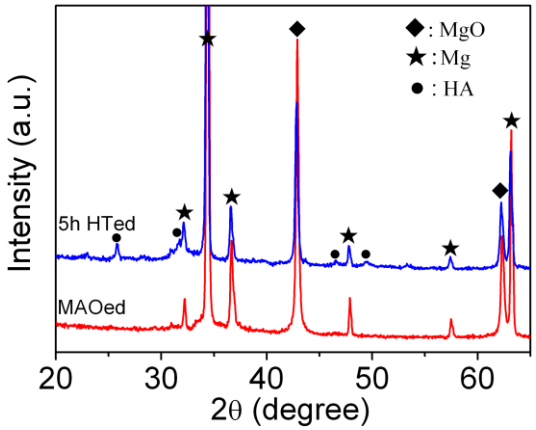

Fig. 1 XRD patterns detected on the surface of MAO_0 coating before and after HT for 5 h.

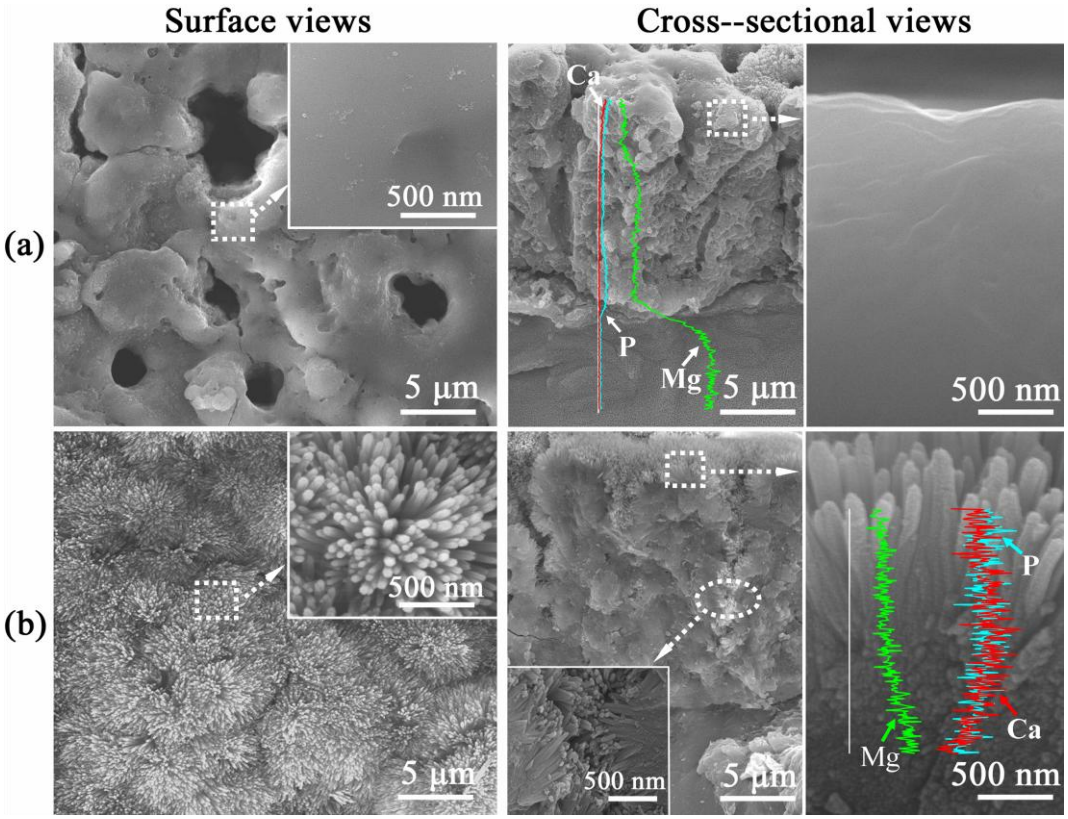

Fig. 2 SEM surface and cross-sectional morphologies of the MAO_0 coating before (a) and after HT for (b) 5 h; the insets are corresponding magnified images of the dotted marked areas.

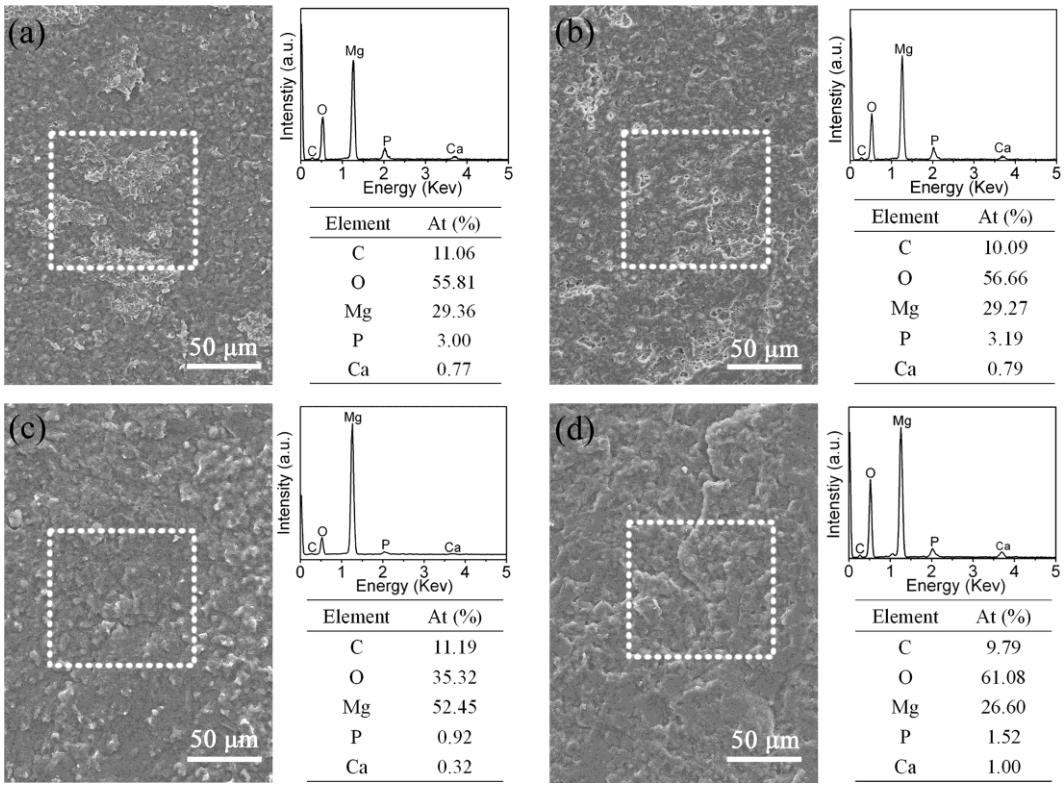

Fig. 3 SEM morphologies as well as EDX spectra and elements contents (right insets) taken from the dotted-squared areas of the tensile fracture surfaces examined on (a, b) MAO_0 and (c, d) HT5h coated Mg; (a, c) the samples sides and (b, d) the steel jigs sides.

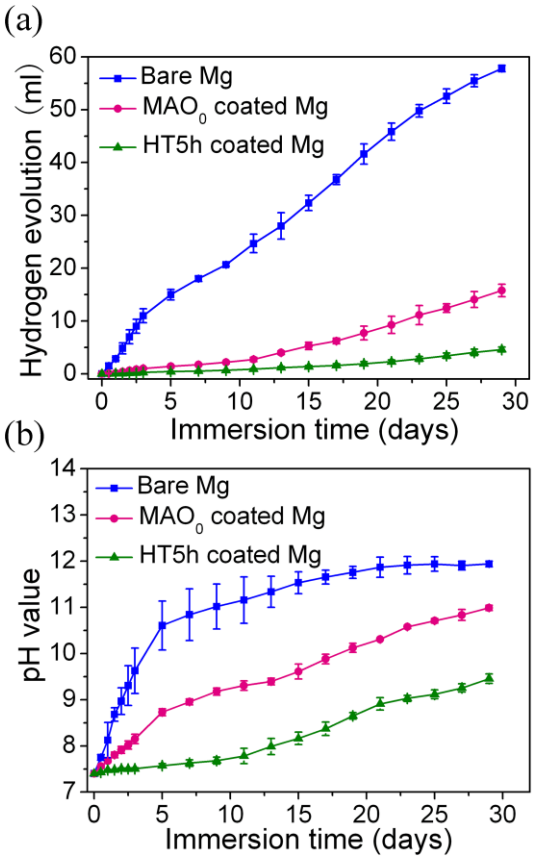

Fig. 4 (a) Hydrogen volumes released by bare and coated Mg in PBS solution and (b) pH values of the PBS solution immersing bare and coated Mg as a function of immersion time.

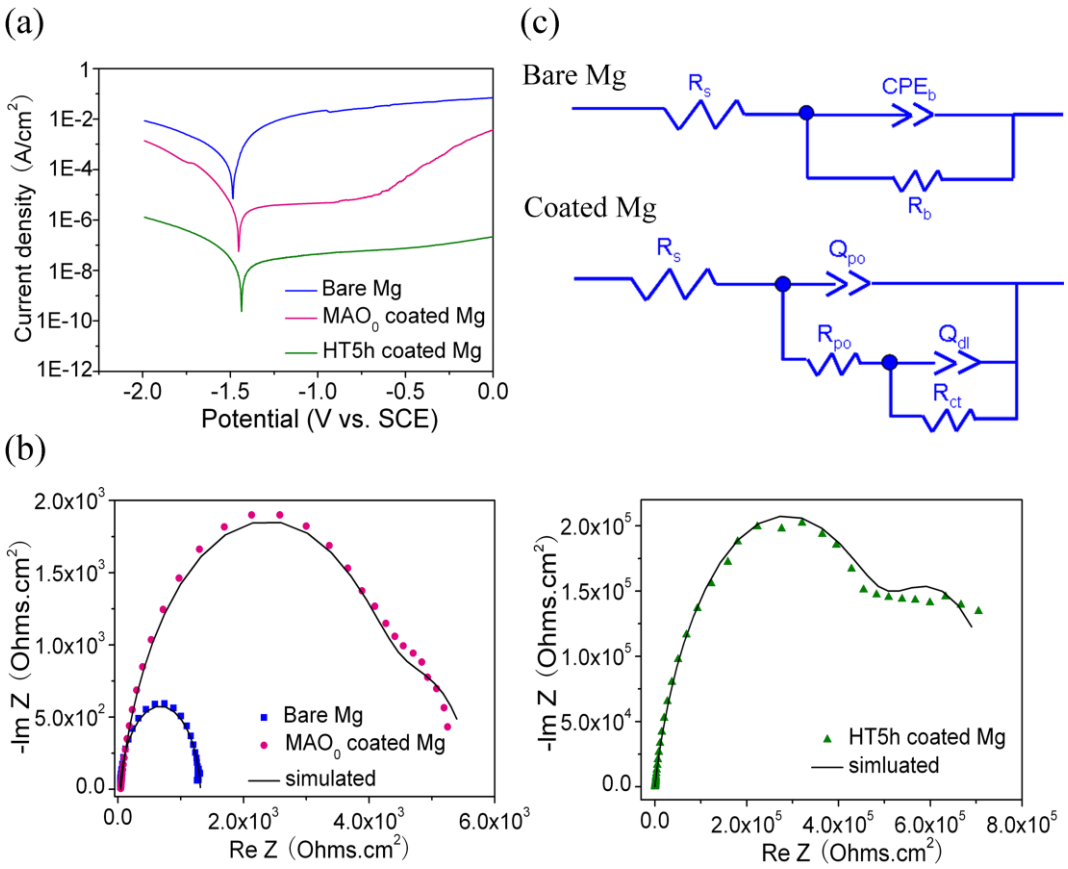

Fig. 5 (a) Polarization curves and (b) Nyquist plots of EIS spectra of bare and coated Mg discs measured in PBS solution, (c) equivalent circuits used to fit the impedance data of bare and coated Mg discs.

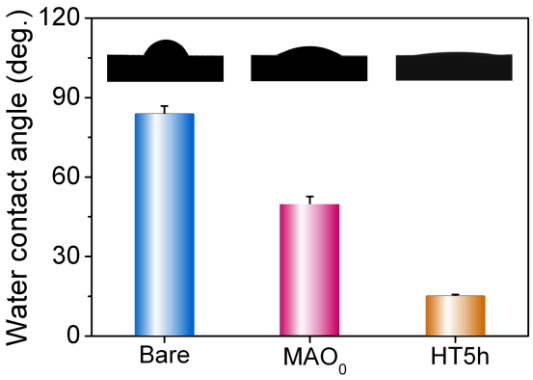

Fig. 6 Hydrophilicity of (a) bare, (b) MAO_0 and (c) HT5h coated Mg.

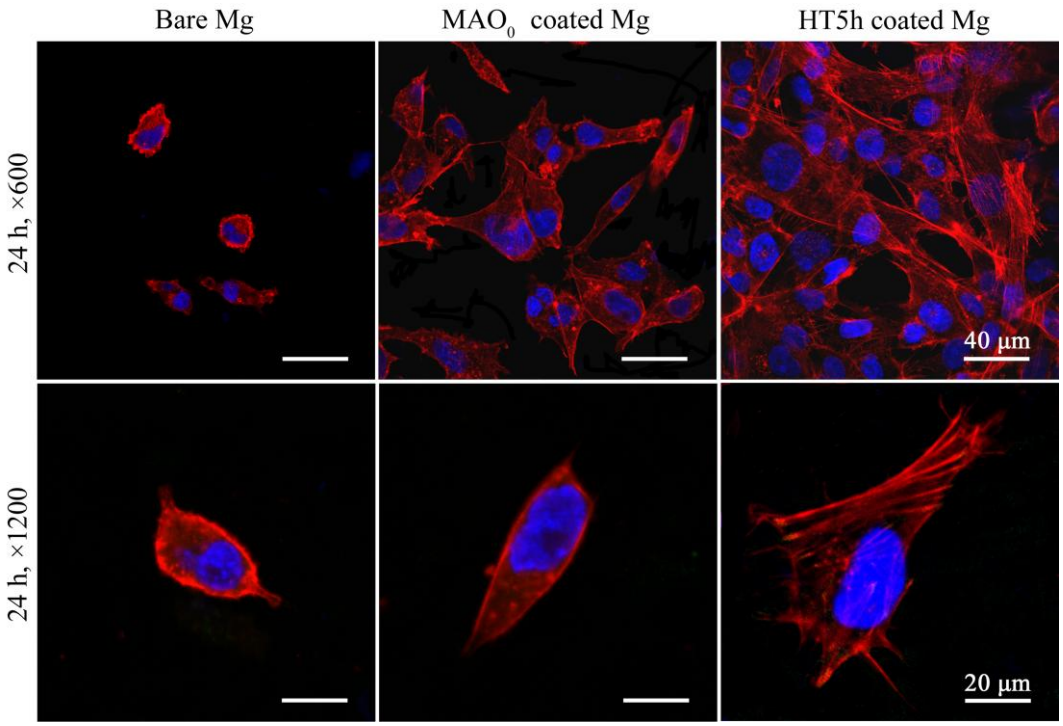

Fig. 7 Actin (red) and cell nucleus (blue) fluorescence images with different magnifications of osteoblast after 24 h of culture on bare Mg as well as MAO_0, and HT5h coated Mg.

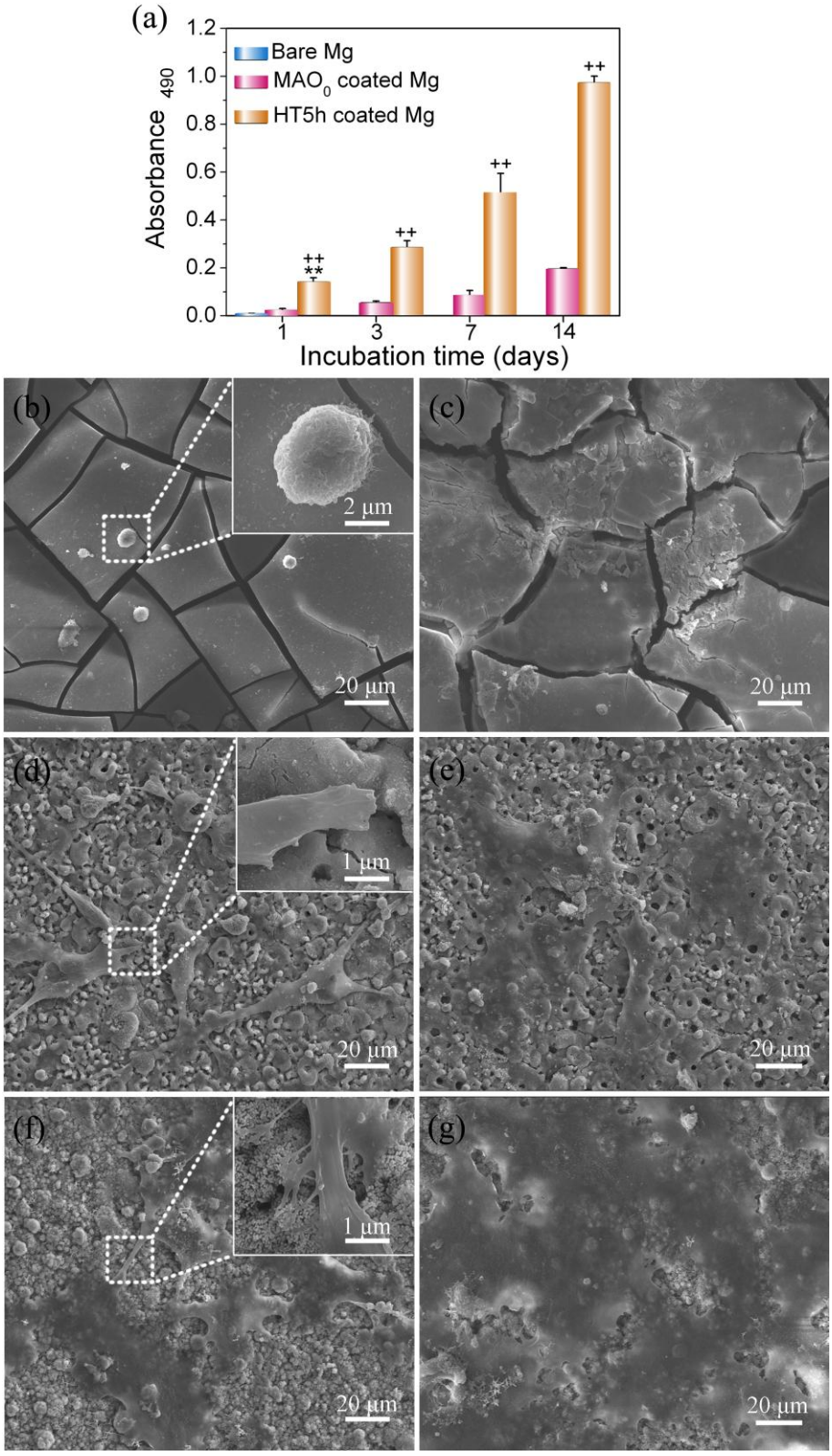

Fig. 8 (a) MTT assay of osteoblast incubated on bare and the coated Mg for 1, 3, 7 and 14 days; SEM morphologies of osteoblast cultured on bare (b, c), MAO_0 (d, e) and HT5h (f, g) coated Mg for 1 day (b, d and f) and 3 days (c, e and g). Data are presented as the mean ± SD, n = 4, (**) $p < 0.01$ compared with the bare Mg, and (++) $p < 0.01$ compared with the MAO_0 coated Mg.